Makri, K., Lockett, R. D., Jeshani, M. & Price, R. (2016). The effect of cavitation on atomization in non-evaporating diesel sprays. Paper presented at the ILASS – Europe 2016, 27th Annual Conference on Liquid Atomization and Spray Systems, 4-7 Sep 2016, Brighton, UK.

CITY UNIVERSITY LONDON

The Effect of Cavitation on Atomization in Non-Evaporating Diesel Sprays

Kassandra Makri[1], Russel Lockett*[1], Mahesh Jeshani[1], Richard Price[2]
[1]Department of Mechanical Engineering & Aeronautics, The City University, London, UK
[2]Shell Global Solutions, Brabazon House, Manchester, UK
*Corresponding author: r.d.lockett@city.ac.uk

Abstract
The determination of the distribution of the local liquid volume fraction (LVF) in non-evaporating diesel sprays was achieved using Laser Induced Fluorescence (LIF). The LVF distribution developing during the primary and secondary atomisation was investigated as a function of rail pressure, physical properties and needle lift. Samples of conventional diesel and light kerosene were injected through an optically accessible mini-sac type injector, employing a custom diesel fuel injection system. The optical arrangement facilitated the acquisition of images with an image resolution of 28μm/pixel using a high speed camera operating at 10 kHz. The analysis is focused on images obtained at different injection stages (1.8ms, 3.7ms, 5.6ms after start of injection (SoI)). The results revealed that the diesel spray developed an asymmetric structure, especially at the intermediate and later stages of the injection. The LVF decreases with increasing axial distance and the primary atomisation occurs immediately after the spray enters the surrounding gas. Lastly, the findings of the phenomenological analysis suggests that conventional diesel shows a later primary and secondary atomisation than light kerosene, due to their difference in the physical properties.

Introduction
The most common processes associated with atomization is the conversion of bulk liquid into a jet or sheet and the growth of disturbances which finally lead to the disintegration of the jet into ligaments and eventually into small droplets. The disintegration or breakup occurs when the disruptive forces exceed the liquid surface tension force. The consolidating effect of liquid surface tension tends to pull a liquid into a form that exhibits the minimum surface energy, while the stabilizing effect of liquid viscosity tends to oppose any change in liquid geometry. External forces (aerodynamic, centrifugal forces etc.) acting on the liquid surface may distort the bulk liquid and promote the disruption [1].
When a liquid jet is injected into another stationary fluid, the competition between the cohesive and the disruptive forces lead to oscillations and perturbations in the liquid. Under particular conditions, the oscillations may be amplified to such an extent that the bulk liquid disintegrates into droplets. This initial breakup is often referred to as primary breakup or primary atomization. A population of larger droplets produced in primary atomization may be unstable if they exceed a critical droplet size and thus may undergo further disintegration into smaller droplets. This process is usually termed secondary breakup or secondary atomization. Therefore, the final droplet size distribution produced in an atomization process is determined by the liquid properties in both primary and secondary atomization. [1]
These processes determine not only the structure, shape and penetration of the resulting spray but also its specific characteristics of droplet velocity and drop size distribution. Spray characteristics are strongly influenced by the nozzle size and geometry, the physical properties of the liquid and gaseous medium into which the liquid jet is discharged. The most important liquid properties are surface tension, viscosity and density. In particular, atomization is a result of the competition between viscous, surface tension forces and the disruptive actions of various internal and external forces. The main factors that affect the atomization process are the turbulence in the liquid flow, cavitation in the nozzle and aerodynamic interaction with the surrounding gas. A liquid jet emanating from a nozzle or orifice exhibits richly varied phenomena that depend on the orifice geometry, the inlet condition before the jet is emanated, and the environment into which the jet is issued. A liquid jet cannot escape the breakup process because of hydrodynamic instability. The breakup possesses two major regimes: large drop formation and fine spray formation. These two regimes are controlled by distinctively different physical forces, and between them there exist intermediate regimes. All the regimes arise from a subtle dynamic response of the jet to the disturbances. [1] The relative contributions of each of these mechanisms and the resulting impact on the spray structure are dependent on many factors including the transient nature of the injection process, the peak injection pressure, the pressure profile, the ambient density, the air motion and turbulence, the nozzle diameter and length, the mini-sac volume and configuration and the finish on internal flow passages. [2]
In general, sprays and other dispersed flows are normally divided into dilute and dense flow regimes, which are both observed in sprays. Dilute dispersed flows contain well-defined dispersed phase elements, e.g. spherical drops or bubbles and have relatively small local dispersed phase volume fractions. In case of the dilute spray drop collisions are infrequent and heat, mass transfer and drag coefficients of individual drops are independent of liquid volume fraction or drop spacing. [3, 4] However, a dilute spray does not correspond to the behaviour of

isolated drops in known conditions, since transport from the drops influence the structure of the continuous phase. The understanding of dilute dispersed flows is established through the application of optical diagnostics and new methods that are suitable for analysing turbulence [5]. Dense dispersed flows are typified by the dense-spray region near the exit of the injector. This region involves the transition between liquid flow in a passage and the dilute dispersion of drops which marks the start of dilute spray region. Thus, large liquid volume fractions are important features of dense sprays. They are characterized by irregularly-shaped, rather than spherical, liquid elements, such as ligaments and the long liquid core associated with pressure-atomized sprays as well as by some other complex phenomena e.g. collisions of liquid elements, effects of liquid volume fraction in interphase transport rates and breakup of liquid elements. [4] There are some difficulties in dense spray measurements due to the need for high spatial resolution and the opacity to optical diagnostics.

Early models of spray breakup were based solely on the interaction between the spray and the surrounding atmosphere. Later, as the importance of the nozzle became evident, spray models included empirical factors to account for the effect of the nozzle. Unfortunately the interaction between the atmosphere and the spray remained unclear, impeding the study of the nozzle-spray connection. Since neither part of the breakup process was completely understood, it was difficult to gauge the relative contribution of the nozzle and the ambient atmosphere to spray breakup. Additionally, the role of the nozzle in spray breakup remained obscure because of the surprising complexity of the internal nozzle flow. Not only has the role of turbulence in the nozzle been investigated, but also the effect of cavitation on high-pressure fuel injection systems as well. This accumulation of understanding emphasizes the role of cavitation in perturbing the flow through the nozzle and the ensuing spray [6]. In particular, Hiroyasu et al. [7] showed that cavitation appeared in enlarged orifice (d=3.00mm) in co-operation with the wall friction lead to disturbances of the jet surface. This disturbance is amplified by the interfacial forces resulting in a short break up length of the core. In more detail, as the injection velocity increases a cavity appears at the nozzle entrance which in turn generates intense turbulence. The turbulent structures of the flow perturb the jet surface at the nozzle exit and as result the break up length of the spray decreases.

Other investigations on the spray break-up [8, 9] are based on electric conductivity measurements of conducting fluids which make use of the conductivity difference between the liquid core and the developing sprays. Their findings suggest the existence of an intact liquid core which eventually disintegrated into small droplets due to aerodynamic effects. However, if only the aerodynamic effects were responsible for the spray break up then the atomisation process would not have been affected by cavitation effects or nozzle geometry. This contradicted the experimental findings of Kano et al. and Gulder et al. [11, 12] who have investigated the effect of cavitation on the atomisation process in diesel fuels and found that there are no long-lived incompletely atomised ligaments or sheets along the spray.

Other authors [10] proposed a break up mechanism which was a result of the synergy between cavitation and aerodynamic interaction of the liquid phase with the surrounding gas. In the vicinity of the nozzle exit there is an undisturbed liquid core; at its edges cavitation bubbles are present which implode when they leave the nozzle hole and air entrainment rises up. The cavitation bubbles are assumed to be generated inside the nozzle hole close to the nozzle entrance and they last for some microseconds in the free jet. The bubble collapse follows, creating disturbances in the emerging spray. These disturbances are responsible for the radial motion of the liquid and the generation of the pressure waves that disintegrate the large liquid droplets, acting in support of the aerodynamic forces. The phenomenological analysis of the sprays revealed that the length of the liquid core was directly proportional to the lifetime of the cavitation bubbles.

Other phenomenological studies on atomization of spray jets showed that primary atomization began when the jet left the nozzle hole [9, 13]. The abrupt change in boundary conditions was believed to enable the radial component of internal jet turbulence to transport fluid elements away from the jet axis, hence facilitating the breakaway of large unstable drops and ligaments from the jet core. It was stated that the core of the spray jet was progressively eroded by internal turbulent flow causing fluid element breakaway [13]. They also expressed a relationship which describes the distance from the jet exit where primary break up occurs.

$$\frac{x_i}{\Lambda} = C_{xt}\left(\frac{\bar{u}_o}{\bar{u}_o}\right)^{9/5} We_{L\Lambda}^{-0.4} \quad (1)$$

or

$$x_i/\Lambda = 3890 We_{f\Lambda}^{-0.67} \quad (2)$$

$$We_{f\Lambda} = \rho_L \Lambda \bar{u}_o^2 / \sigma \quad (3)$$

Cheroudi et al. [9] have estimated the length of the intact core (L_c) of the spray.

$$\frac{L_c}{d} = C_C \left(\rho_L / \rho_g\right)^{1/2} \quad (4)$$

In this work, the authors carry out a phenomenological analysis of atomisation in cavitating spray jets of two fuels, un-additised crude oil and light kerosene, at two rail pressures, 250 bar and 350bar, in order to highlight the significant effect of cavitation on the atomization process. There is no significant amount of other studies which have utilised Laser Induced Fluorescence to quantify the Liquid Volume Fraction (LVF) of diesel sprays.

Material and methods

Fuels preparation

The fuels utilised for the purposes of this experiment are identified by A and B and were provided by Shell Global Solutions. Fuel A is a middle distillate diesel, while Fuel B is a light kerosene. The physical properties of the fuels are shown in Table 1.

Table 1: Physical properties of fuels A, B.

Fuel type	Physical properties			Boiling point range
	Density (kg/m^3)	Kinematic Viscosity (mm^2/s,@40°C)	Surface Tension (mN/m)	Celsius degrees (°C)
fuel A	825	2.078	31.39	170-350
fuel B	803	1.664	28.46	150-210

In order to take measurements of the fluorescence, the incident laser light to the emerging spray must be within the absorbance spectrum of the dye. The closer the excitation wavelength was to the peak absorption wavelength of the tracer the greater the excitation efficiency. Rhodamine-B (RhB) was selected to be the fluorescent dye for these experiments, with an excitation wavelength of 527 nm and broadband emission wavelength of 570 nm – 590 nm. However, the RhB powder was not readily soluble in diesel; therefore a solvent with similar boiling point to the fuels was chosen to dissolve the dye prior to addition to the fuels. The selected solvents were 1-Decanol and 1-Octanol for Fuel A and Fuel B respectively. The concentration of RhB in the stock solution was 0.6g/L, which was then mixed with diesel/kerosene using a 1:4 vol/vol ratio (stock solution:fuel) to produce a final solution with a dye concentration of 0.12g/L.

Experimental setup- Fuel injection system-optical arrangement

Rhodamine B doped fuel was delivered into a Denso injector using a custom diesel common rail fuel injection system. The fuel delivery system can generate injection pressures up to 700bar and inject a precisely determined amount of fuel at a predetermined rate. The high pressure fuel supplied to the common rail pressure accumulator was injected into the surrounding atmosphere each time the injector was opened. The needle lift had a constant lift rate of 0.118 mm/ms for approximately 4ms, followed by a time period of 0.3ms in which the needle reached its maximum lift, followed by a 1.6ms time period of needle return. The needle returned to its initial position at approximately 6ms after the electronic start-of-injection signal.

The fuel was injected through the nozzle holes with a forward angle of 25 deg through an optically accessible mini-sac type six-hole acrylic nozzle tip. The dimensions of the acrylic tip were a precise replica of a conventional nozzle tip (D~140μm, L~1mm, L/D=7.5). The excitation of RhB at 527nm was achieved using a Nd:YLF laser operating at 10 kHz (New Wave Research Pegasus-PIV dual head laser). The laser beam was formed into a laser sheet approx. 20mm high and 0.2mm wide at the focal point, using a 1.0 m focal length spherical lens, and a 6x cylindrical telescope (-25 mm and +150 mm cylindrical lenses).

One of the six spray jets emanating from the nozzle tip was intersected by the laser sheet, producing laser Mie scattering and laser induced fluorescence. A Photron FASTCAM SA1.1 high-speed video camera was connected to a Nikon 85 mm f1.4 camera lens, reverse coupled to 65 mm extension tubes. This imaging system facilitated an image resolution of approximately 28µm/pixel and an optical magnification of 0.7. For the experimental acquisition, the lens was set to f1.4, and the camera was configured to image 1024x512 pixels acquired at a frame rate of 10 kHz, an exposure of 370 ns, and a dynamic range of 12 bits (0-4095). During the experiments the camera was set to acquire 100 frames (10ms) per acquisition pulse. This produced approximately 17 frames prior to injection, 50 frames (5.0ms) during the injection and 33 frames post injection. The spray entered the object field of view of the camera 3 mm downstream of the nozzle exit (22 nozzle diameters downstream of the nozzle exit).
Figure 1 shows a simplified schematic of the customised common rail diesel fuel injection system, while Figure 2 shows the arrangement of the camera and collection optics relative to the spray being imaged.

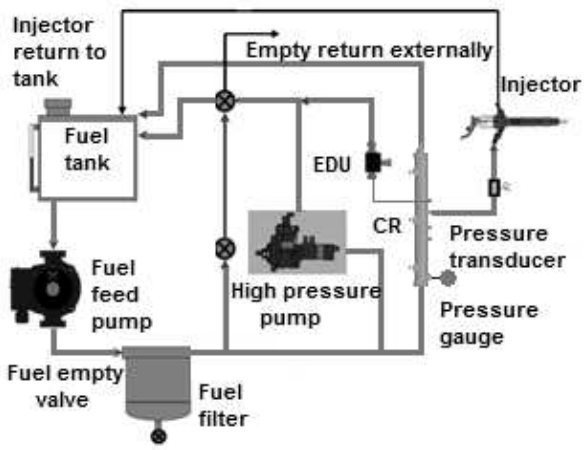

Figure 1. Schematic of fuel injection system.

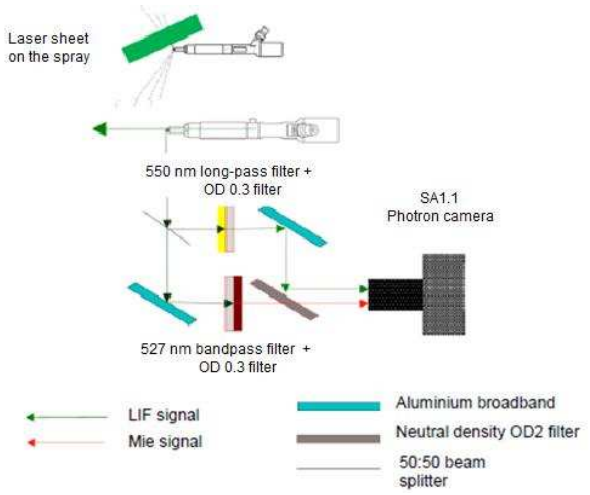

Figure 2. The LIF/Mie scattering two-channel imaging setup

Data processing

Laser Induced Fluorescence (LIF) images

The injection of one of the diesel fuel samples into air, operating at common rail pressures of 250 bar and 350 bar was conducted during each experimental test. Image data were collected from 100 and 65 successive injections in the case of fuel A and fuel B respectively. The camera was set to acquire 100 frames per injection event at 10 kHz for 10ms duration. Hence, each experimental set consisted of 10,000 images for fuel A and 6,500 images per fuel, per rail pressure.
The 1024 x 512 images acquired from the camera contain LIF and Mie images as is shown in Figure 3. Prior to the experiment, a range of background images were obtained which was used to produce the mean background image. The mean background image was then subtracted from the experimental images and the resultant image split into two halves of 512 x 512 pixels each. The left half of the images corresponded to the LIF images and the right hand images to the Mie images.

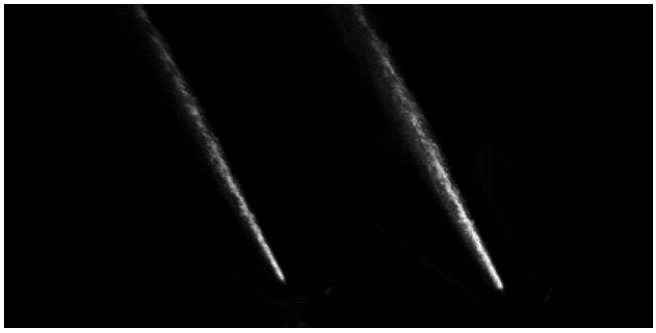

Figure 3. A LIF-MIE combined image captured in the LSD camera showing LIF scattering from the dye on the left and Mie scattering from the spray on the right hand side. The dashed line represents the split of the image into two halves.

The intensity of the pixel located on the CCD chip at the position defined by the row index i and the column index j; iϵ{0,1,2 … ,512}, jϵ{0,1,2 … ,1024} was denoted by S_{ij}^{klm}. The frame number was represented by index *k* within a set of 100 images for a single injection event, ranging from frame 1 to frame 100; while the specific injection

event was represented by the index number *l* and lies between the range of injection 1 and injection 100 for fuel A and injection 1 to injection 65 for fuel B. The index number *m* referred to the diesel fuel sample tested, namely A or B.

A set of 1000 background images were obtained for each experimental session. B_{ij}^{mq} represents the indexed intensity value where the index numbers i, j and m stand for row, column indices and diesel fuel sample as described above. Index number *q* refers to background image 1 to 1000. A mean background image was produced for each experimental set. This is expressed by eq.5.

$$\overline{B_{ij}^{m}} = \frac{1}{1000}\sum_{q}^{N} B_{ij}^{mq} \quad (5)$$

The mean background subtracted image was represented as I_{ij}^{klm} and was equal to $S_{ij}^{klm} - \overline{B_{ij}^{m}}$. I_{ij}^{klm} was then split into two halves, LIF_{ij}^{klm} and Mie_{ij}^{klm}. For the purposes of this work, only the LIF_{ij}^{klm} images are subjected to further processing. The obtained LIF images were corrected against the Gaussian profile of the laser in order to eliminate any possible artefacts in the images.

This process was utilised to eliminate the light sensitivity characteristics of every single pixel in the image. This is illustrated in eq. 6.

$$LIF_{ij,corr}^{klm} = \frac{LIF_{ij}^{klm} - \overline{B_{ij}^{m}}}{\text{Gaussian laser profile} - \overline{B_{ij}^{m}}} \quad (6)$$

In addition, the mixture calibration was important as the fluorescence yield of the fluorophore changes depending on their solution they were dissolved in. The work here required 2 sets of mixture calibrations, i.e. Rhodamine B (RhB)-decanol mixture in diesel (Fuel A identified below as FDD), and RhB-octanol mixture in kerosene (Fuel B identified below as FOLD). The sheet forming optics were removed. After the measurements were obtained, the laser power was measured using a power meter to be able to calibrate the final yield profile against laser power. A mean of 1000 calibration images was determined, and then compared with each other, with the RhB mixture in diesel Fuel A as the baseline benchmark.

The averaged calibration ratios are shown in Table 2. Ultimately, the corrected LIF images of Fuel B (RhB-octanol-kerosene (FOLD)) were divided by 1.04, so the image intensity obtained from the two fuels were comparable, and could be used to determine local Liquid Volume Fraction (LVF).

Table 2. Fluorescence yield calibration ratios for the fluorescent yield of RhB mixtures.

FDD/FDD	FOLD/FDD
1	1.04

A set of instantaneous mean LIF images were obtained from $LIF_{ij,corr}^{klm}$ for a set of *l* = 100 injections in the case of fuel A and *l* = 65 injections in the case of fuel B. This involved calculating the mean images, to be obtained from image frames 1, 101, 201,… 9901; 2, 102, 202,…, 9902 and so on up to frame 100, 200,…, 10,000 for fuel A, and similarly frames 1, 101, 201,… 6401; 2, 102, 202,…, 6402 and so on up to frame 65, 165, 265,…, 6500 for fuel B. Frames 23, 42 and 61 are used for the purpose of this analysis. These frame numbers correspond to the beginning of needle lift (1.8ms after SoI), the maximum needle lift (3.7ms after SoI) and the return of the needle lift (5.6ms after SoI) for each injection. All the images were rotated by -25 degrees so the spray appeared vertical.

The largest LIF signal was obtained along the central axis of the 250bar spray obtained from Fuel A. The mean top 1% of the pixel intensities was utilised to normalise the data and obtain a LIF/LVF value of 1.0. The LIF signal provides information for the local LVF; the normalised pixel data in the range of 0.0 - 1.0 intensity provides direct information about the LVF across the whole length of the spray. Hence, the obtained results for both fuels and rail pressures are relatively comparable to each other. Figure 4 shows a single shot normalised LIF image obtained from a fuel A, 250bar spray at 3.8ms after SoI. The field of view shows the spray 3.0mm downstream of the nozzle exit to 18mm downstream the nozzle exit.

Figure 4. A single shot normalised LIF image from a fuel A spray at 250 bar. (Captured at 3.8ms after SoI)

Phenomenological analysis of the emerging sprays

In order to perform the phenomenological analysis of the sprays, it was necessary to estimate the distance from the nozzle exit where primary break-up begins and the length of the liquid core of the spray. This analysis was based on the analysis of Faeth *et al.*[13]. The same authors [13] argued that the location of the onset of primary break-up is described by eq.2. The location where primary break-up occurs was found from the distance required for the critical size turbulent eddy to move from the jet exit and form a drop as a result of Rayleigh break-up of the corresponding protruding eddy-sized ligament. In order to calculate the distance from the nozzle exit where primary breakup is evident, it is essential to have an estimation of the radial spatial integral scale of turbulence, Λ. According to the same authors Λ is equal to one eighth of the jet diameter, (i.e $\Lambda = \mathrm{dj}/8$). From the optical observation of the emerging sprays for both fuels and rail pressures, it was observed that the diameter of the jet increased with increasing axial distance from the nozzle exit; hence, it was essential to obtain information of the jet diameter along the spray axis.

The diameter of the jet immediately downstream of the nozzle exit is equal to the diameter of the nozzle hole (ø~140μm). However, the optical arrangement for these experiments enables the imaging of the spray from 3mm to 18mm downstream of the nozzle exit. However, the focus of this analysis was on the spray starting 1mm from the nozzle exit up to 4mm downstream. Thus, the spray jet diameter between 0mm and 3mm was estimated, using a linear interpolation between the initial jet diameter and the one obtained from the LIF images, 3 mm downstream of the nozzle.

A Matlab code developed at City University was employed for the determination of the jet diameter at various points along the spray. Initially, a binary mask was applied onto the single shot LIF_{corr} image in order to exclude any scattering effects which may have been present around the spray structure. Then, a low threshold of 10% of the local maximum intensity was applied to the images to eliminate the noise and the artefacts found in them. After the thresholding, 20 equally spaced points were defined along the edges of the first 5mm (8mm from the nozzle exit) of the spray. The diameter of the jet was defined as the radial distance between the point on the left edge of the spray and the corresponding point on the right spray. This procedure was repeated for frame 23, 42, 61 over 100 and 65 injections in cases of fuel A and fuel B, respectively. The obtained 20 x 100 and 20 x 65 matrices contained information about the jet diameter at the 20 pre-determined points for fuel A and fuel B respectively; the mean jet diameter value was calculated for each point and the resultant mean values were used for the rest of the analysis.

The mean jet diameter values were used to calculate Λ and $We_{f\Lambda}$ and these in turn were used in eq.3 in order to calculate the location of the onset of primary breakup (x/Λ).

Liquid Volume Fraction (LVF) distribution along the spray central axis

The determination of the LVF distrubution of the emerging spray along the central axis was obtained using a Matlab code developed at City University. Initialy, the LIF_{corr} images were subjected to binning process in order to obtain smoother spray edges. The resultant image was a mean image produced by the mean values obtained by a 10 x 10 pixel sliding window which scanned every single pixel of the images under examination. Then, the pixels with intensity lower than 10% of the maximum intensity detected along the central axis, were eliminated in order to ensure that the obtained signal did not correspond to noise or image artefacts. The obtained image was then converted into a binary image which was applied as a mask onto the initial LIF_{corr}. Hence the latter image contained only information that met the above criteria.

This was followed by the determination of the mid-points of the upper and lower edges of the sprays, together with the spray centreline. The centreline was two pixels wide and its length matched with the length of the spray in each image. The profile of the LVF distribution along the central axis was plotted against the axial distance from the nozzle exit (3mm - 18mm).

Spray asymmetry of the developed diesel sprays

The optical observation of the raw data revealed that there is a strong asymmetry in the sprays, especially in case of fuel A. For this purpose, a Matlab code developed at City University facilitated the accurate determination of the central axis which is at first utilised to split the spray structure into three horizontal segments and then to split these sections into two equal divisions. A 10 x 10 pixel sliding window was utilised to overcome the problem of the pixelated spray edges; the resultant images have much smoother spray borders. Then, a binary mask was applied on the smoothened images to eliminate any artefacts or scattering effects which might be present around the main spray structure. The obtained masked image was then scanned row by row to detect the pixel in which the intensity is equal to the 10% of the local maximum intensity found in each row; subsequently, it is reasonable to argue that the low threshold applied to each image under examination is equal to the 10% of the local maximum intensities found along the spray structure. Thus, any value below the local low threshold was set to zero. After the thresholding, the images were subjected to a 2D linear interpolation, in order to construct new data points within the range of the discrete set of the known pixel intensities in each frame. The refinement factor was set to 3. This meant that the intervals (pixels) of the refined grid (image) was repeatedly divided by 3 in each dimension; consequently each pixel of the initial image was split into 9 sub-pixels. Then, the code precisely calculated the mid-points along the spray, determining the half-way point of the number of pixels found in each row of the spray.

Once the mid-points were determined the code fitted a linear curve (central line of the spray) to the mid-points which had a R^2 value above 0.96 in all cases. The code then split the spray body into three horizontal equal divisions, the upper, middle and lower segments. Each division was then divided into two equally spaced segments. Consequently, the spray was divided into six equal segments and the distribution of the LVF was calculated for each segment.

Results and discussion

Mean diesel LVF distribution along the spray central axis – Fuels A, B at 250bar and 350bar

Figures 5a, 5b, and 5c show the graphs of the centre-line LVF distribution as a function of the axial distance from the nozzle exit. In more detail, they show the LVF profile of the central axis obtained after 1.8ms, 3.7ms, 5.6ms after the SoI for fuel A (solid line) and fuel B (dotted line) at 250 bar (black) and 350 bar (grey). A visual comparison of the figures 5a, 5b, 5c show that the LVF of the spray central axis reaches its maximum value at around 3.6 mm downstream from the nozzle exit while it reaches its minimum value at around 18 mm from the orifice. This observation suggests that the liquid core does not survive up to the point of 3mm; it is either destroyed between the 0mm and 3mm or it never exited the nozzle, due to intense cavitation phenomena occurring inside the nozzle hole. However, in figure 5b it can be seen that in case of fuel A at 350 bar, the curve reaches a plateau approximately between 3.4mm and 4.1 mm downstream the nozzle exit, suggesting the existence of a liquid core. It should be also noted that the maximum LVF values obtained for fuel A and B are around 0.8 and 0.62 respectively. This discrepancy is a consequence of the different viscosity and surface tension between the two fuels. Additionally, the comparison of the graphs reveals that the decaying rate of the LVF along the central axis is slightly lower in of fuel A relative to fuel B, due to later primary and secondary atomisation. Lastly, it is observed that the LVF profiles obtained at 250 bar and 350 bar for both fuels seem to follow the same trend, irrespectively of the pressure increase.

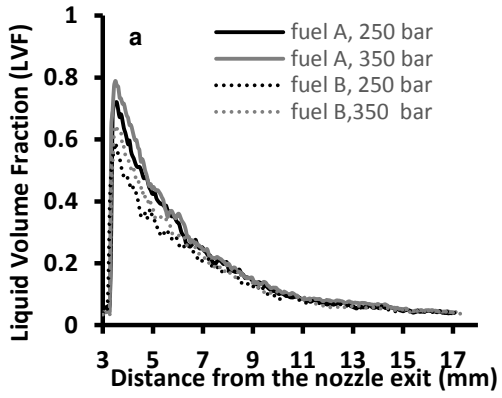

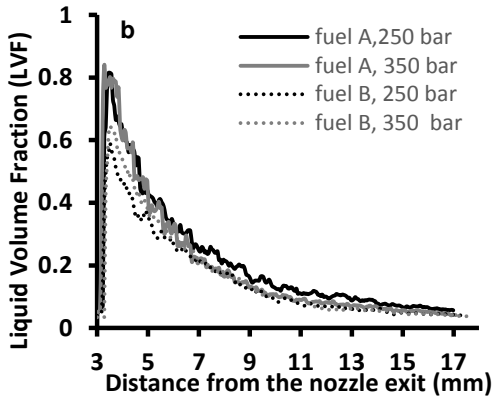

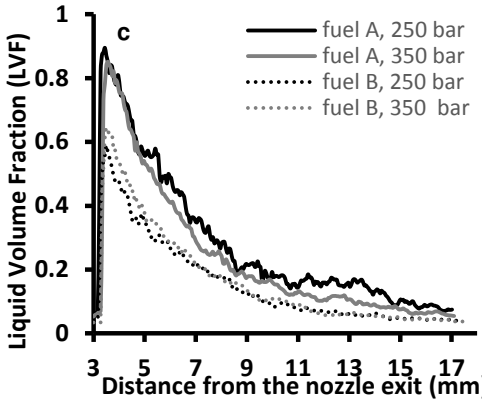

Figure 5. Graphs of centre-line mean diesel LVF with distance at a) 1.8ms, b) 3.7ms and c) 5.6ms after the SoI in cases of fuels A, B at 250bar and 350 bar.

Laser Induced Fluorescence – Fuel A at 250bar and 350 bar

1.8 ms after SoI

Figure 6 shows two graphs of the normalised frequency as function of LVF for the upper (solid line), middle (dashed line) and the lower (dotted line) segments of the spray and the left hand side (black) and right hand side (grey) of each segment. Both graphs are projections of the normalised histograms which represent the number of pixels in each segment of the mean normalised LIF image. The obtained LVF values lie in the range of 0.0 to 1.0 in 45 distinct divisions. Applying the above mentioned methodology, the area under each curve is equal to 1. Figure 6a, and 6b depicts that the LVF of the droplets decreases with increasing axial distance from the nozzle exit. This finding is expected as the spray is denser close to the nozzle exit, while further downstream it becomes more dispersed due to the effect of secondary atomization. It is also shown that in the vicinity of the nozzle exit, the obtained LVF distributions are wider than the ones produced for the upper segments. This is a consequence of the larger population of liquid ligaments close to the orifice due to primary atomization. On the contrary, further downstream of the nozzle exit, the atomised spray is a result of the synergy of primary and secondary atomization; the resultant finer droplets have a lower LVF value. The comparison of the left hand side and the right hand side distributions appear to be fairly similar to each other, suggesting that the spray developed in a quite symmetric manner. Lastly, it is also observed that the trend of the obtained curves in all cases at 250 bar and 350 bar is the same, which indicated that at this point the pressure does not seem to have a significant impact on the LVF values.

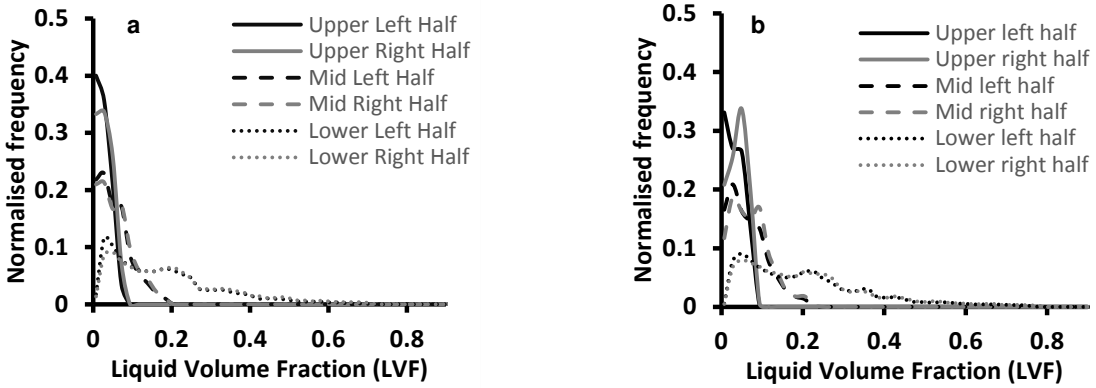

Figure 6. Graph of normalised frequency of the upper, middle, lower segments of the a) 250 bar and b) 350 bar spray, as a function of LVF at 1.8 ms after SoI.

3.7ms after SoI

Figure 7 shows two graphs of the normalised frequency as function of LVF for the upper (solid line), middle (dashed line) and the lower (dotted line) segments of the spray and the left hand side (black) and right hand side (grey) of each segment.

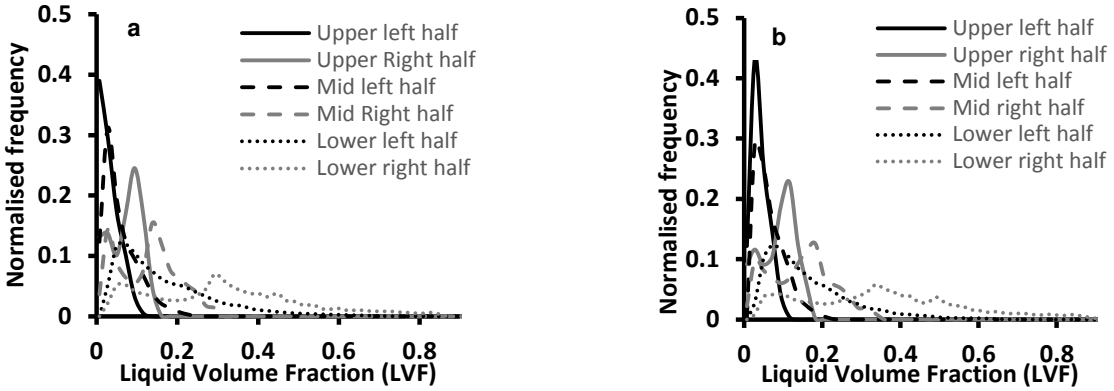

Figure 7. Graph of normalised frequency of the upper, middle, lower segments of the a) 250 bar and b) 350 bar spray, as a function of LVF at 3.7 ms after SoI.

The LVF is normalised against the top 1% of the LVF values observed in case of fuel A at 250bar, so the distributions shown in figure 7 are comparable to the ones in figure 6. A visual comparison of the left hand and the right hand side of the spray in all the three cases (lower, middle, upper segments) suggests that the spray have developed in a strongly asymmetric manner. In particular, the right hand side distributions contain droplets with larger LVF values than the ones in the left hand side of the spray in all segments at both pail pressures. It is believed that the observed spray asymmetry is a consequence of the geometric cavitation appearing at the same side at the nozzle hole entrance. The overall distributions shown in figure 7 show that the larger LVF values are present close to the nozzle exit, resulting to broader distributions than the ones obtained at the middle and upper segments. Additionally, the curves produced for both rail pressures seem to follow the same trend.

5.6ms after SoI

Figure 8 shows the projections of the normalised histograms obtained at the upper, middle, lower spray segments and provide information about the LVF distribution at the left hand side and right hand side of each spray segment. The various line styles and colors retain their meaning as defined above. In this case, the spray appears to be less asymmetric than in case of spray captured at 3.7ms after SoI, but the asymmetry is still quite significant. Comparing the distributions produced for 250 bar and 350 bar, it can be stated that the distributions become narrower with increasing rail pressure. This is probably a consequence of the flow dynamics induced by location of the needle at this particular moment, 5.6ms after SoI (the needle is about to seal). Moreover, the LVF of the droplets decreases with increasing axial distance from the nozzle exit.

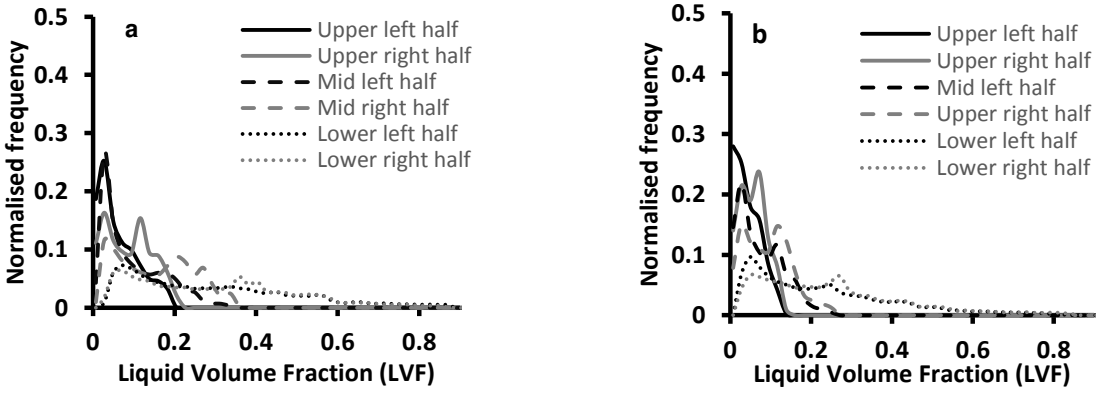

Figure 8. Graph of normalised frequency of the upper, middle, lower segments of the a) 250 bar spray and b) 350 bar spray, as a function of LVF at 5.6 ms after SoI.

Laser Induced Fluorescence – Fuel B at 250bar and 350 bar

1.8 ms after SoI

Figure 9 shows two graphs of the normalised frequency as function of LVF for the upper (solid line), middle (dashed line) and the lower (dotted line) segments of the spray and the left hand side (black) and right hand side (grey) of each segment. Both graphs are projections of the normalised histograms which represent the number of pixels in each segment of the mean normalised LIF image. The obtained LVF values lying in the range of 0.0 to 1.0 in 45 distinct divisions. Applying the above mentioned methodology, the area under each curve is equal to 1.

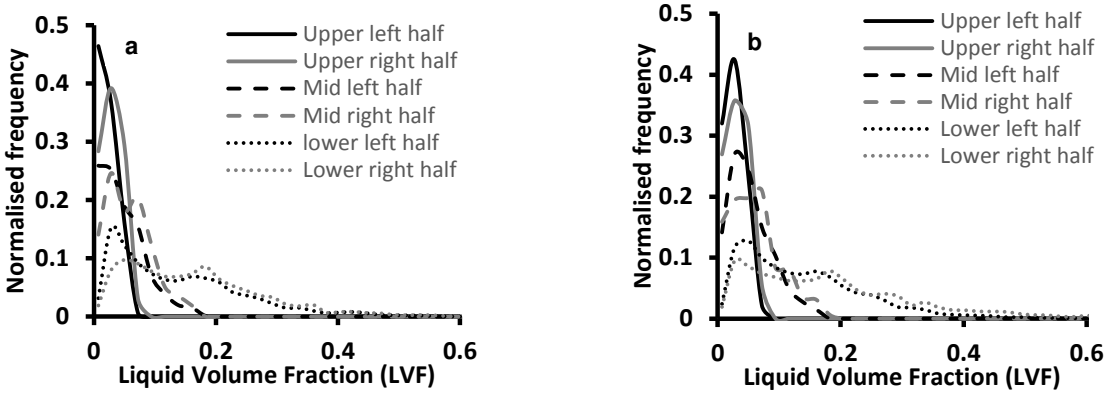

Figure 9. Graph of normalised frequency of the upper, middle, lower segments of the a) 250 bar spray and b) 350 bar spray, as a function of LVF at 1.8 ms after SoI.

The distributions obtained from the left hand side of the spray segments compared with the ones from the right hand side show that fuel B spray developed in a much more symmetric way than fuel A. However, the asymmetry remains, but is less distinctive. The right hand side spray segments contain droplets with slightly larger LVF values. The comparison of figure 9a and figure 9b reveals that the produced curves seem to follow the same trend, irrespectively of the pressure increase. Moreover, in the vicinity of the nozzle exit the LVF distributions are shown to be wider with respect to the ones produced for the middle and upper segments, due to the less pronounced effect of secondary atomization at this region. Lastly, a visual comparison of figures 6 and 9 shows that fuel B produces much narrower distributions than fuel A. This can be attributed to the difference in physical properties (viscosity, surface tension) between the two fuels, resulting in later primary atomisation and secondary atomisation in fuel A relative to fuel B.

3.7 ms after SoI

Figure 10 shows two graphs of the normalised frequency as function of LVF for the upper (solid line), middle (dashed line) and the lower (dotted line) segments of the spray and the left hand side (black) and right hand side (grey) of each segment. The LVF is normalised against the top 1% of the LVF values observed in case of fuel A at 250bar, so the distributions produced in all cases can be comparable to each other.

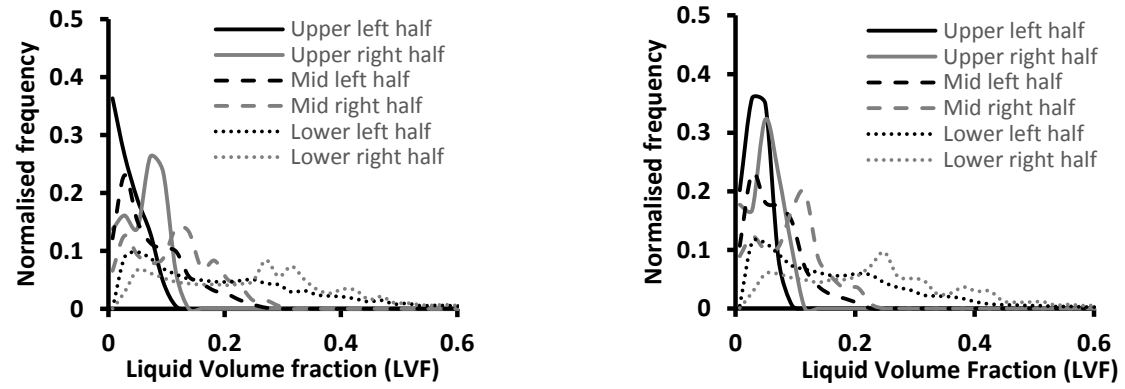

Figure 10. Graph of normalised frequency of the upper, middle, lower segments of the a) 250 bar spray and b) 350 bar spray, as a function of LVF at 3.7 ms after SoI.

A visual comparison of the left hand and the right hand side of the spray in all the three cases (lower, middle, upper segments) suggests that the spray have developed in an asymmetric manner. In particular, the right hand side distributions contain droplets with larger LVF values than the ones in the left hand side of the spray in all segments at both pail pressures. Comparing the distributions produced for 250 bar and 350 bar, it can be stated that the distributions become slightly narrower with increasing rail pressure. A consideration of the graphs in figures 10a and 10b enables a same conclusion as for all the cases examined so far. The largest LVF values are located close to the nozzle exit, followed by the intermediate and the upper segments.

5.6 ms after SoI

Figure 11 shows the projections of the normalised histograms obtained at the upper, middle, lower spray segments and provide information about the LVF distribution at the left hand side and right hand side of each spray segment.

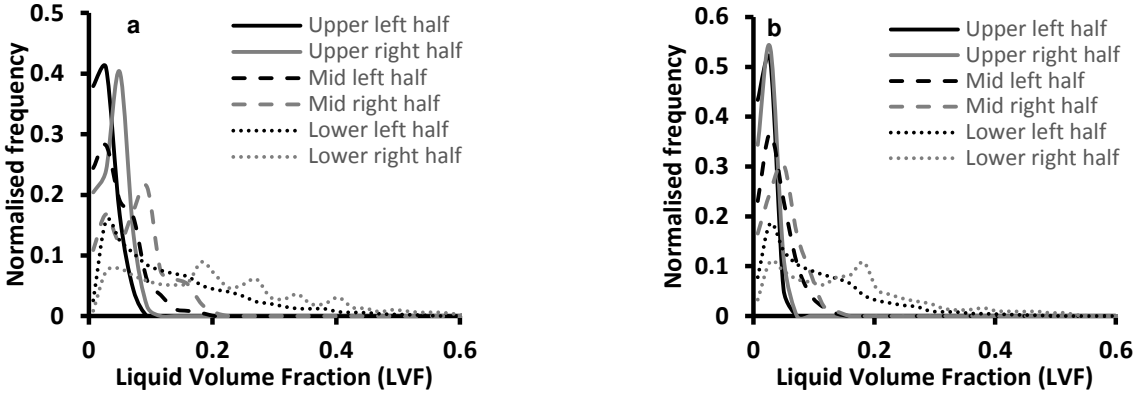

Figure 11. Graph of normalised frequency of the upper, middle, lower segments of the a) 250 bar spray and b) 350 bar spray, as a function of LVF at 5.6 ms after SoI.

In this case, the spray appears to be even more symmetric than in case of spray captured at 3.7ms and 1.8ms after SoI. Comparing the distributions produced for 250 bar and 350 bar it can be stated that the distributions become narrower with increasing rail pressure. A consideration of the graphs in figures 11a and 11b enables a same conclusion as for all the cases examined so far. The largest LVF values are located close to the nozzle exit, followed by the intermediate and the upper segments.

Phenomenological analysis of the sprays

Table 3 shows the results of the phenomenological analysis of both fuels at 250 bar and 350 bar. This analysis is focused on the spray developed between 1mm and 4mm downstream the of the nozzle exit, as this region contain the largest LVF values in all cases; hence primary atomisation most likely occurs somewhere in this spray region. The obtained results show that primary atomisation starts in the vicinity of the nozzle exit, but much earlier form what other authors [13] suggested in their work. The main reason behind this finding is the presence of cavitation in sprays produces for this work. The highly cavitating flow accelerates the disintegration of the liquid spray body and ligaments into finer droplets, not only when the fuel is injected into the surrounding gas but also when it is still inside the nozzle passage. This statement further supports our previous arguments on the short life time of the liquid spray cores. Additionally, a comparison of the results in Table 3 reveals that the onset of primary atomisation is delayed in fuel A relative to fuel B. This can be attributed to the difference in physical properties of the two fuels; an observation made previously as well, when fuel B produced much narrower distributions than fuel A.

Table 3. Axial distance from the nozzle exit where primary atomisation occurs.

Fuel type	250 bar	350bar
	Distance where primary breakup occurs, x (mm)	Distance where primary breakup occurs, x (mm)
fuel A	0.74	0.81
fuel B	0.75	0.73

Conclusions

The conclusion drawn from this work are listed below:

1. Laser Induced Fluorescence is a useful tool for obtaining quantitative measurements of local liquid volume fraction and for determining the onset of primary atomisation.
2. The LVF distributions obtained for the fuel A, B sprays showed to contain larger LVF values in the vicinity of the nozzle exit, while further downstream LVF is gradually decreases due to the more pronounced effect of secondary atomisation.

3. The produced LVF distributions of the two diesel sprays reveal that the sprays developed in a quite asymmetric manner. This asymmetry is more profound at the intermediate and later stages of the injection event and especially in case of fuel A at 350 bar.
4. The LVF values obtained in the spray produced by fuel A were much smaller than the ones obtained in the fuel A spray, suggesting that the onset of primary atomisation in fuel A occurs later than fuel B, due to the lower viscosity and surface tension in fuel B relative to fuel A. This statement is further supporting from the finding of the phenomenological analysis of the two sprays.
5. The LVF profile along the central axis of the sprays along with the results of the phenomenological analysis suggest that the life time of the liquid core is very short, as a consequence of the intense cavitation phenomena occurring inside the nozzle passages, with only an exception in case of fuel A at 350 bar, where there is an indication that the liquid core lasts up to approximately 4.0 mm downstream of the nozzle exit.

Acknowledgements
The authors would like to acknowledge Shell Global Solutions, who provided the financial support for this work, and Mr G. Clow and Mr J.Ford of City University for their technical support.

Nomenclature
C_{xt}: Empirical constant (depends on the nozzle geometry)
C_c: Empirical constant
d : Nozzle passage diameter [mm]
L_c : Intact liquid core [mm]
We: Weber number
X_i : Distance from the nozzle exit [mm]
ρ_L: Density of liquid phase [kg/m^3]
ρ_G: Density of gas phase [kg/m^3]
σ: Surface tension of the liquid phase [Pa s]
Λ: radial spatial integral scale of turbulence [mm]
$\bar{u}_o$: Injection velocity [m/s]
$\bar{\tilde{u}}_o$: Cross-stream rms velocity [m/s]

References
[1] Lefebvre, A., 1988, "Atomization and sprays", Vol. 1040, CRC press.
[2] Dumouchel, C., 2008. On the experimental investigation on primary atomization of liquid streams. Experiments in fluids, 45(3), pp.371-422.
[3] Chigier, N.A., 1976. The atomization and burning of liquid fuel sprays. InEnergy Combust. Science, 2, pp. 97-114).
[4] Chatwani, A.U. and Bracco, F.V., 1985, Computation of dense spray jets, Princeton Univ., NJ (USA). Dept. of Mechanical and Aerospace Engineering.
[5] Ruff, G.A., Sagar, A.D. and Faeth, G.M., 1989, Structure and mixing properties of pressure-atomized sprays, AIAA journal, 27(7), pp.901-908.
[6] Schmidt, D.P., Rutland, C.J. and Corradini, M.L., 1997. A numerical study of cavitating flow through various nozzle shapes, 971597, SAE Technical Paper.
[7] Hiroyasu, H., Shimizu, M., July 1991, Break-up Length of a Liquid Jet and Internal Flow in a nozzle, 5th International Conference on Liquid Atomization and Spray Systems (ICLASS).
[8] Reitz, R. D., and Bracco, F. V., 1982, Mechanism of Atomization of a Liquid Jet, Phys. Fluids, 25(2), pp. 1730-1741
[9] Cheroudi, B., Chen, S.H., Bracco, F.V., and Onuma, Y., 1985, On the Intact Core of Full-Cone Sprays, 850126, SAE Technical Paper.
[10] Fath, A., Munch, K. U., and Leipertz, A., 1997, Spray Break-Up Process of Diesel Fuel Investigated Close to nozzle exit, Int. Journal of Fluid Mech. Res.,24 (1-3).
[11] Kano, H., Kato, M., Kojina, T., and Katagiri, M., 1990, Contribution of Optimum design for nozzle configuration to spray formation, 900824, SAE Technical Paper.
[12] Gulder, O. L., Smallwood, D. L., and Snelling, D.R., 1992, Diesel Spray Structure Investigation by Laser Diffraction and Sheet Illumination, 920577, SAE Technical Paper.
[13] Faeth, G.M., Hsiang, L.P., and Wu, P. K., 1995, Structure and breakup properties of sprays, Int. J. Multiphase Flow, 21 (1), pp.99-127.